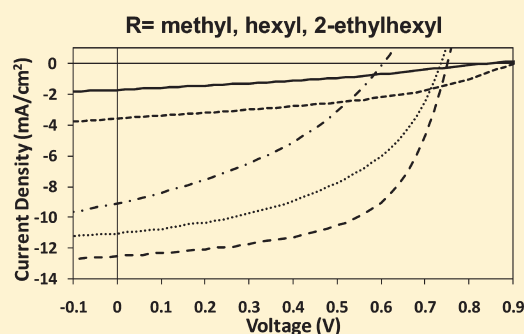
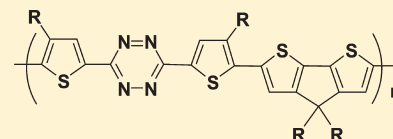


Alternating Copolymers of Dithienyl-*s*-Tetrazine and Cyclopentadithiophene for Organic Photovoltaic ApplicationsZhao Li,^{*,†} Jianfu Ding,^{*,†} Naiheng Song,[†] Xiaomei Du,[†] Jiayun Zhou,[‡] Jianping Lu,[‡] and Ye Tao[‡][†]Institute for Chemical Process and Environmental Technology (ICPET) and [‡]Institute for Microstructural Sciences (IMS), National Research Council of Canada (NRC), 1200 Montreal Road, Ottawa, ON, Canada K1A 0R6

ABSTRACT: As a new emerging electron deficient building block, *s*-tetrazine (Tz) shows high electron affinity, which is even higher than the commonly used benzothiadiazole units. This property makes Tz a very promising electron withdrawing unit for low band gap conjugated polymers, especially for organic solar cell materials. We report the synthesis and property of five alternating copolymers of *s*-tetrazine and cyclopenta[2,1-*b*:3,4-*b'*]dithiophene (CPDT), which are bridged with a thiophene unit. Methyl, hexyl, and/or 2-ethylhexyl groups are introduced onto thiophene and CPDT units to tune the solubility, UV absorption, frontier molecular orbital energy levels, and interchain stacking property of the resulting polymers. These polymers are stable up to 220 °C and decompose to dinitrile compounds with the breaking of Tz linkage at a higher temperature. Efficient bulk heterojunction solar cells were fabricated by blending these polymers with (6,6)-phenyl-C₇₁-butyric acid methyl ester (PC₇₁BM), and they reached a power conversion efficiency up to 5.53% under simulated AM 1.5 G irradiation of 100 mW/cm². The morphological structures of the active layers from different polymers or under different processing conditions were then analyzed by atomic force microscopy (AFM) and correlated with their device performance.

KEYWORDS: *s*-tetrazine, low band gap, conjugated polymer, bulk heterojunction, solar cell



INTRODUCTION

As one of the most electron-deficient C–N heterocycles, *s*-tetrazine (Tz)-containing compounds have drawn much research attention recently because of their unique properties.¹ First, although the Tz ring has a small size, it renders unusually high electron affinity in its aromatic compounds, which makes Tz an ideal building block for electro-optically active materials. For example, Tz compounds have been used as sensing or fluorescent materials² and are even claimed to be the world's smallest organic fluorophores.³ Second, Tz derivatives have a very high nitrogen content. These nitrogen atoms provide multiple binding sites and can be employed in coordination chemistry for metal complexation,^{1c} and some other Tz compounds have been intensively studied as explosive materials, which have remarkably high energy content.⁴ Third, the Tz ring shows high reactivity as a diene in cycloaddition reaction; thus, Tz has been used as precursor for some new pyridazines or natural products using the Carboni–Lindsey reaction.⁵ However, up to now, most of these studies are focused on small molecular compounds because of the absence of an efficient synthetic approach for the formation of Tz based polymers. Wiggins and Pasquinet et al. reported the synthesis of Tz-based unconjugated linear or hyperbranched polymers.^{6,7} Grote et al. attached Tz to ion-exchange resin as side chains to modify its anion-exchange properties toward precious metal ions.⁸ Audebert et al. reported the first example of an electroactive conjugated polymer containing a Tz moiety in each

repeating unit.⁹ However, this polymer was prepared by electrochemical polymerization, so the resulting material is insoluble in organic solvent. Thus, detailed investigation of its properties and application is difficult.

Recently, we reported the synthesis of the first solution-processable Tz backboned conjugated copolymer, PCPDTTTz.¹⁰ Its main chain contains alternating Tz and CPDT units bridged by thiophene (Figure 1). This kind of structure is unique for polymers and especially for conjugated polymers because the conjugation through Tz is introduced into the main chains, instead of the commonly used –C=C– bond. The simple and straightforward synthetic approach opens a door for the preparation of various Tz-containing conjugated polymers and allows us to carry out detailed studies on their structure and property relationship. More importantly, efficient polymer solar cells have been obtained by blending these polymers with (6,6)-phenyl-C₇₁-butyric acid methyl ester (PC₇₁BM), demonstrating an important application of these novel electro-optically active materials.¹¹

Benzothiadiazole (BT) is one of the most commonly employed electron withdrawing building blocks because of its very strong electron-deficient property. High efficiency polymer solar cells were fabricated by several groups on the basis of its polymers.¹² To compare the effect of Tz and BT moieties, we

Received: February 1, 2011

Revised: March 1, 2011

Published: March 17, 2011

synthesized two polymer analogues with the structures shown in Figure 1.¹⁰ Interestingly, as compared with the energy levels of the BT polymer (PCPDTTBTT), both the highest occupied molecular orbital (HOMO) and the lowest unoccupied molecular orbital (LUMO) energy levels of the Tz polymer (PCPDTTTz) became much lower, with the values reduced by 0.25 and 0.12 eV, respectively. This led to a larger open circuit voltage (V_{oc}) of the photovoltaic devices when using PCPDTTTz-based devices (0.75 V) than when using PCPDTTBTT-based devices (0.56 V).¹³ In addition, it also resulted in a slightly broader band gap (1.86 vs 1.73 eV).

Following our previous study,¹⁰ in this work, we synthesized several bisthieryl-s-tetrazine (TTz) monomers with a methyl, hexyl, or 2-ethylhexyl side group on the 4-position of the thiophene ring. These electron-deficient monomers were then copolymerized with electron-rich cyclopenta[2,1-b:3,4-b']dithiophene (CPDT) monomers to obtain low band gap polymers. We investigated their thermal decomposition, optical, electrochemical, and chain packing properties, and compared their performance in solar cell devices.

RESULTS AND DISCUSSION

Monomer and Polymer Synthesis. The bisthieryl-s-tetrazine (TTz) monomer synthesis starts from 4-alkyl-2-thiophene carboxaldehyde, which can be synthesized from 3-alkyl thiophene by reacting with *n*-butyl lithium and then 1-formylpiperidine

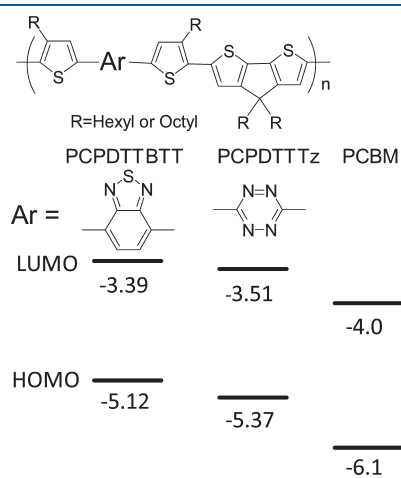


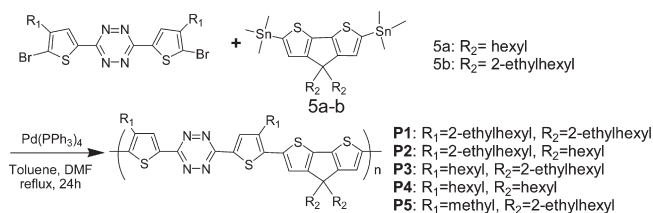
Figure 1. Structures and energy levels of PCPDTTBTT, PCPDTTTz, and PCBM.

(Scheme 1). However, this approach will inevitably produce about 12% isomer (3-alkyl-2-thiophene carboxaldehyde). It is difficult to remove from the product at this stage. We noticed that to use lithium 2,2,6,6-tetramethylpiperidide (LiTMP) instead of *n*-butyl lithium will improve the selectivity of the reaction.¹⁴ We found that this 3-substituted isomer will not interfere with the next step reaction for the formation of the nitrile compound, and it can be completely removed from the desired product at this stage by a careful column chromatography. A modified sulfur-assisted Pinner synthesis was employed to prepare the symmetrical alkyl substituted dithienyl-s-tetrazine (TTz),¹⁵ where the thiophene nitrile was treated with hydrazine in the presence of sulfur to form 1,4-dihydro-s-tetrazine, which was then oxidized to s-tetrazine by isoamyl nitrite. We noticed that the size of alkyl groups has a steric effect for this reaction, as the alkyl increases from hydrogen, methyl, hexyl, to 2-ethylhexyl; the yield of this ring-closing reaction decreased from 60% to 45%, to 41%, and then to 36%.^{15c} These TTz compounds can then be easily brominated to corresponding dibromide monomers.

Cyclopenta[2,1-b:3,4-b']dithiophene (CPDT) has been successfully used to prepare high performance polymer solar cell materials and has been demonstrated as an efficient electron-rich unit;¹⁶ thus, it was chosen as the comonomer unit in this work. The trimethyltin CPDT monomer was prepared as reported,^{16a} which was then copolymerized with the above TTz monomers by the Stille coupling reaction to yield five polymers with different side chain combinations (Scheme 2). As shown in Table 1, after careful purification by solvent extraction, the average molecular weight (M_n) of the polymers ranged from 11.9 to 29.4 kDa, with the polydispersity index (PDI) ranged from 1.50 to 2.14.

As expected, the solubility of these polymers improves with increasing content of the branched alkyl chain. For example, polymers **P1** and **P3** can be dissolved in chloroform, chlorobenzene, THF, and *o*-dichlorobenzene (*o*-DCB) at room temperature, while **P2** and **P5** are only soluble in these solvents at an elevated temperature. **P4** can be only dissolved in chlorobenzene

Scheme 2. Synthesis of the Conjugated Polymers



Scheme 1. Synthesis of the Tetrazine Monomers

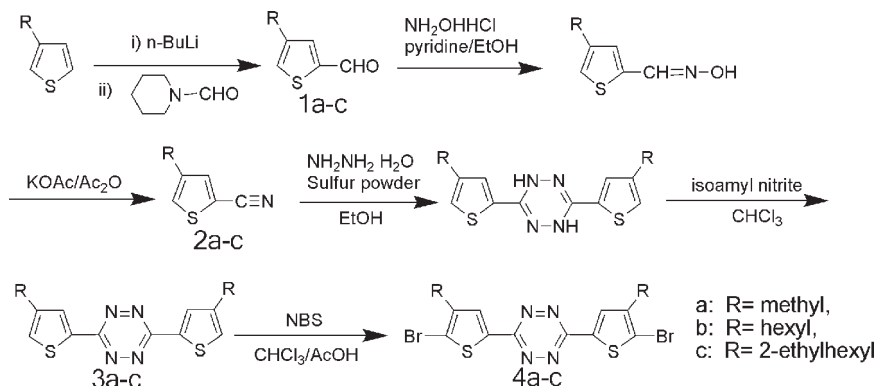


Table 1. Polymer Characterization

polymers	M_n (kDa) ^a	PDI ^a	soln λ_{\max} (nm) ^b	film λ_{\max} (nm)	E_g^{opt} (eV) ^c	$E_{1/2}^{\text{red}}$ (V) ^d	$E_{1/2}^{\text{ox}}$ (V) ^d	LUMO (eV) ^e	HOMO (eV) ^e
P1	17.0	2.00	546	551	1.72	-0.87	0.94	-3.53	-5.34
P2	11.9	2.14	563	577	1.61	-0.88	0.95	-3.52	-5.35
P3	29.4	1.51	562	560	1.66	-0.88	0.95	-3.52	-5.35
P4	20.0	1.41	588	590	1.60	-0.89	0.97	-3.51	-5.37
P5	15.6	1.50	564	575	1.60	-0.94	0.86	-3.46	-5.26

^a Average molecular weight number and polydispersity index (GPC vs polystyrene standards in chlorobenzene). ^b Solution absorption in chlorobenzene. ^c Optical energy gap estimated from the onset of the UV curve measured in thin film. ^d Half wave potentials from CV measurements of thin films in a 0.1 M Bu₄NPF₆/CH₃CN solution vs Ag. ^e Estimated from $E_{\text{LUMO}} = -(E_{1/2}^{\text{red}} + 4.40)$ eV and $E_{\text{HOMO}} = -(E_{1/2}^{\text{ox}} + 4.40)$ eV.

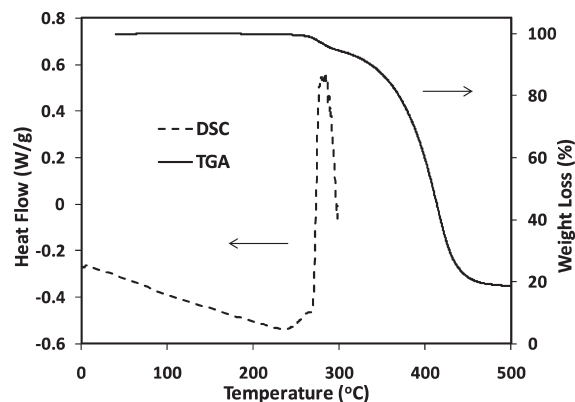


Figure 2. DSC and TGA curve of polymer P4 with a heating rate of 10 °C/min in nitrogen.

or *o*-DCB at higher temperatures. It is interesting that P3 shows better solubility than P2, although both of them bear two hexyl and two 2-ethylhexyl groups in each repeat unit but at different positions. This indicates that whether the branched alkyl chains are on the thiophene or CPDT units will significantly affect the solubility and interchain stacking. It appears that the branched alkyl chains on the CPDT units can create stronger steric hindrance for chain stacking than these on the thiophene units when these two branched chains are crowded on the same carbon in the fused triple-ring coplanar structure of CPDT.

Thermal Stability and Decomposition. The thermal stability of the polymers was investigated with differential scanning calorimetry (DSC) and thermal gravimetric analysis (TGA). Typical DSC and TGA curves of P4 are shown in Figure 2. The DSC analysis showed that the polymers are all stable up to 220 °C, while a huge exothermic peak appeared with an onset at 250 °C. The TGA curve also showed about 4% weight loss between 250 and 300 °C. We noticed that the dark blue polymer solid changed to yellow oil after a scan from 0 to 300 °C, indicating an occurrence of dramatic chain scission of the polymer. ¹H and ¹³C NMR spectra of this yellow oil showed that a highly pure dinitrile (compound 6 in Scheme 3) was obtained even without any purification (Figure 3), and its FT-IR spectrum gave a strong peak at 2214 cm⁻¹, which was attributed to nitrile group. GPC analysis of the resulting yellow liquid revealed a main decomposition product with a monomodal distribution (PDI = 1.03) and M_n of 720 g/mol (inset of Figure 3). This result agrees with the decomposition species displayed in Scheme 3 and confirms the decomposition route of the polymer, where the Tz unit decomposed to nitrile with release of N₂ gas and cleavage of the remaining N–N bond. This

agrees well with previously suggested decomposition pathways of small molecular 3,6-substituted *s*-tetrazines.¹⁷ This decomposition reaction may be employed to prepare symmetric dinitrile compounds.¹⁸

Optical Study and X-ray Diffraction. The UV–vis spectra of the polymers in chlorobenzene solution and in thin solid film are shown in Figure 4, and the corresponding data are summarized in Table 1. All polymer solutions show high molar absorptivity (ϵ_{max}) from 4.4×10^4 to 5.6×10^4 (M⁻¹ cm⁻¹). Comparatively, the solid films show slightly broader absorption peaks, and the maximum absorption peaks only have a small red shift (less than 14 nm) as compared with those of the solution spectra. Interestingly, P4 displays an absorption peak at the longest wavelength in the five polymers, with a red shift of about 25 nm in solution and 13–39 nm in solid film when compared with the others. Its solution also has the highest molar absorptivity, and the UV curve contains a small shoulder near 680 nm, indicating some aggregation even in the dilute solution. Because P4 contains all linear hexyl side chains, we believe this red shift was caused by stronger interchain interaction due to lower steric hindrance from the side groups on thiophene and CPDT units for chain stacking. In this regard, one might suggest that P5 should have even smaller steric hindrance because there is only a methyl group on the thiophene bridge as compared with that of the hexyl or 2-ethylhexyl groups for the other polymers, but in fact P5 has a UV absorption maximum located between those of P4 and the other polymers. This result, once again, proved that the branched 2-ethylhexyl groups on the CPDT unit have more significant steric hindrance than that on the thiophene bridge.

X-ray diffraction (XRD) curves of these polymer films are shown in Figure 5. Polymers P1 to P4 all have a broad peak at 2θ of 6.6°, corresponding to an interchain distance of 15.5 Å, while only P4 shows a clear and broad π – π stacking peak at 2θ of 27°, corresponding to a short π – π stacking distance of 3.8 Å. This result agrees well with our previous discussion that P4 has stronger interchain stacking than the other polymers.

Electrochemical Properties. The cyclic voltammetry (CV) curves of these polymer thin films on the platinum electrode coated with chlorobenzene solution are shown in Figure 6, and half wave potentials are summarized in Table 1. All polymers show reversible electroactive properties. Polymers P1 to P4 have similar oxidation and reduction potentials at 0.95 and -0.88 V, respectively, versus the Ag quasi-reference electrode. So the HOMO and LUMO energy levels were calculated to be -5.35 and -3.52 eV with an electrochemical band gap of 1.83 eV, which is slightly larger than their optical band gaps (1.60–1.72 eV). Comparatively, polymer P5 shows raised HOMO and LUMO energy levels at -5.26 and -3.46 eV. It is interesting

Scheme 3. Thermal Decomposition of Polymer P4

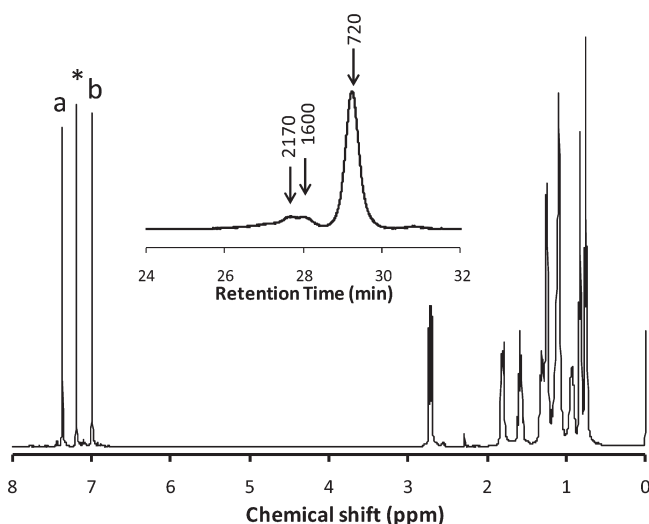
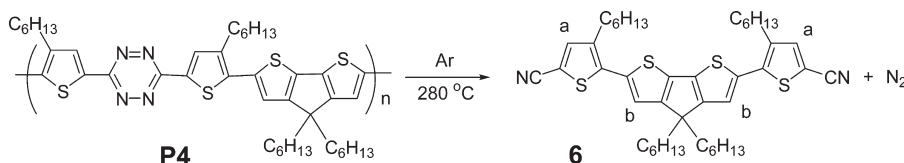


Figure 3. ^1H NMR spectrum (in CDCl_3) of the crude product from the thermal decomposition of **P4**, see Scheme 3 for peak assignment. (Inset: GPC curve of the crude product; the molecular weights of corresponding peaks are shown with an arrow).

that the replacement of hexyl or 2-ethylhexyl with the methyl group on the thiophene bridge has such an effect on their electrochemical properties.

Photovoltaic Performance. Bulk heterojunction solar cells were fabricated with a general structure of ITO/PEDOT-PSS (40 nm)/polymer:PC₇₁BM(100 nm)/LiF(1 nm)/Al. As reported in our previous paper,¹⁰ **P4** produced an optimized device performance with a short-circuit current density (J_{sc}) of 12.5 mA/cm^2 , a V_{oc} of 0.75 V, a FF of 59%, and a PCE of 5.53%, under the following device processing condition: polymer/PC₇₁BM ratio of 1/2, DIO content of 3.0%, and spin-coating temperature of 80 °C (device **D4**). Similar processing conditions were applied to the other polymers (**D1** for **P1**, **D2** for **P2**, **D3** for **P3**, and **D5** for **P5**). Figure 7a compares the current density–voltage (J – V) curves of these five devices, with the device fabrication conditions and performance data summarized in Table 2. Among these five devices, device **D4** (from **P4**) has the best performance with the data listed above. Device **D5** (from **P5**) shows the lowest V_{oc} (0.60 V) in the five devices, about 0.15 V lower than that of **D4**, agreeing well with the CV results (Table 1). It should be noted that although device **D1** and **D3** have higher V_{oc} , their J_{sc} values are extremely lower. This is probably due to the poor film morphology formed in the active layers. As mentioned above, polymers **P1** and **P3** have the best solubility and are soluble in o-DCB even at room temperature. The combined effect of the good solubility of the polymer and the enhance solubility of PC₇₁BM due to the use of the processing additive, 1,8-diiodooctane (DIO), might hamper the phase separation during spin-

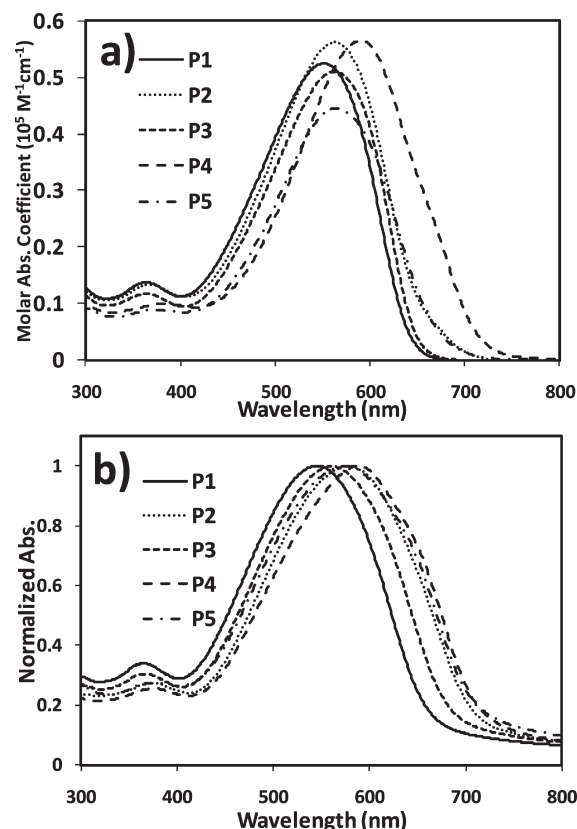


Figure 4. UV absorption spectra of dilute solutions in chlorobenzene (a) and thin films (b) of the polymers.

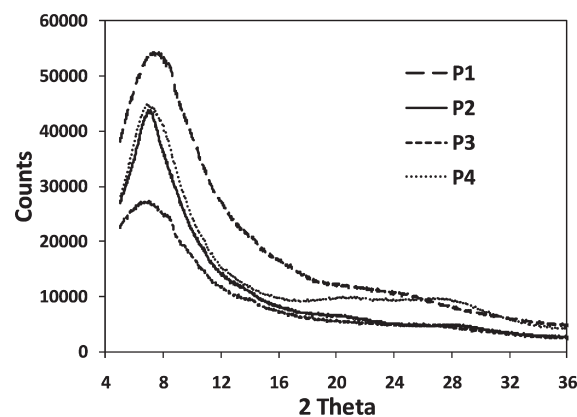


Figure 5. XRD spectra of the polymer films.

coating, resulting in a poorly phase-segregated active layer. Therefore, **P1** and **P3** were also fabricated at room temperature without using DIO to generate **D6** and **D7** in order to obtain a

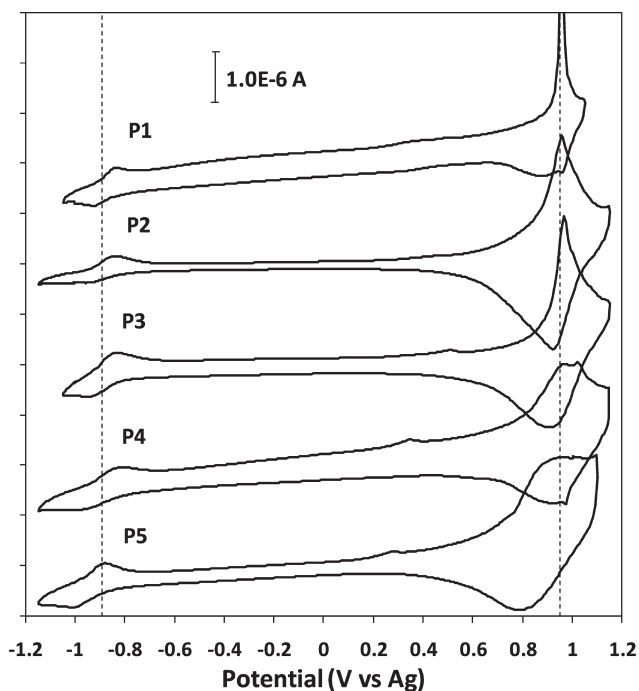


Figure 6. Cyclic voltammograms of polymer films on the platinum electrode in $\text{Bu}_4\text{NPF}_6/\text{CH}_3\text{CN}$ solution.

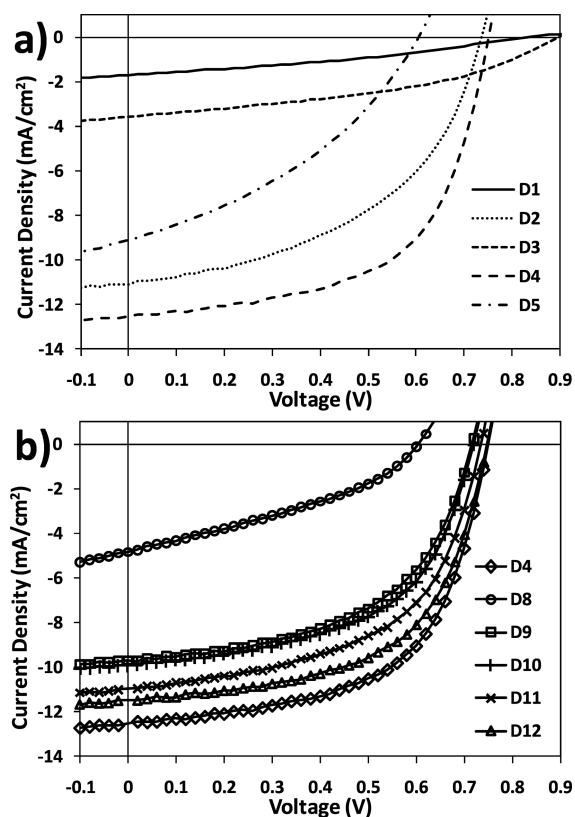


Figure 7. J - V curve of (a) polymer: PC_{71}BM (weight ratio 1:2) bulk heterojunction solar cells and (b) $\text{P4}:\text{PC}_{71}\text{BM}$ solar cells under a simulated AM 1.5 G irradiation of 100 mW cm^{-2} .

better phase separation. The resulting devices showed better performance than those fabricated at elevated temperature using

DIO (D1 and D3), indicating a better morphological structure in D6 and D7. Intrigued by this result, we also prepared a device from P4 without using DIO; the obtained device (D8) showed a much poorer performance than that of D4. This contradicted result of the DIO effect for the polymers with poor and good solubility indicates that the effect of DIO on the device performance depends on the solubility and chain-stacking capability of the individual polymer. To further explore the DIO effect, devices with different amount of DIO (0.0%, D8; 1.3%, D12; 3.0%, D4, and 4.5%, D12) were fabricated from P4. The results showed that the best performance was still from D4, while devices D11 and D12 also performed well. This result indicates that DIO is beneficial in creating a better morphological structure for P4. Different weight ratios of P4 to PC_{71}BM (1/1 for D10; 1/2 for D4; 1/3 for D9) were also tested, and their J - V curves were compared in panel (b) of Figure 7. It is shown that these three devices have similar V_{oc} and FF values, while the J_{sc} value of D4 is much better than those of D10 and D9, indicating that a ratio of 1:2 of P4/ PC_{71}BM gives the best balance in light absorption and charge transport, as is proved in the following discussion.

The external quantum efficiency (EQE) spectra of devices D10, D4, and D9 from polymer P4 with weight ratios of 1:1, 1:2, and 1:3, respectively, are compared in panel (a) of Figure 8, while the corresponding UV absorption spectra of the active layers are shown in panel (b) of Figure 8. As listed in Table 2, the integrated J_{sc} from the EQE spectra agrees well with the data from the J - V curves. The EQE of D4 reaches 60% from 450 to 600 nm, while that of D10 covers a broader range from 400 to 650 nm at over 50%. D9 shows a lower EQE from 400 to 700 nm because of the lower polymer weight ratio that resulted in a limited light absorption. These results prove the importance of the weight ratio between donor and acceptor, which will also influence the morphological structure of the resulting bicontinuous network for balancing the electron and hole transport.

Atomic Force Microscopy (AFM). The surface morphological structure of the active layer of the polymer/ PC_{71}BM blend was analyzed by tapping mode AFM (Figure 9). The films on D6 and D7 show obscure domains without clear phase separation, corresponding to the modest FF of 30.2% and 38.4%, respectively. The films on D2 and D9 have a clear interpenetrated two-phase morphology, while the film on D9 shows a finer structure. This may explain the better performance of D2 and D9 among these devices. Large scale ($5 \mu\text{m} \times 5 \mu\text{m}$) images of the film on D8 show large round domains with sizes over 100 nm, which apparently indicates the formation of large spherical crystals of the polymer or PC_{71}BM during spin-coating (Figure 9g,h). Interestingly, besides these big domains, other regions of the image still show a phase-segregated structure (Figure 9i,j). We believe that this is caused by the mismatched crystallization rates of the polymer and PC_{71}BM during the spin coating. PC_{71}BM tends to precipitate and crystallize faster than P4; thus, large PC_{71}BM islands formed first during spin-coating at a high temperature. These islands span across the film and might act as defects in the device and limit interfacial area between the two phases, which might explain why the device performance of D8 is so poor. DIO has a higher boiling point than the host solvent, *o*-DCB, and shows good solubility only for PC_{71}BM , and during spin coating, DIO will evaporate slower than *o*-DCB. So, its addition will decrease the tendency of precipitation and crystallization of the PC_{71}BM phase to match with that of P4;¹⁹ thus, better phase segregation can be expected as in D9 (Figure 9k,l).

Table 2. Summary of the Device Fabrication Conditions and Device Performance

devices	polymer/PC ₇₁ BM w/w ratio	DIO ^a (%)	temp ^b	J_{sc} ^c (mA/cm ²)	V_{oc} (V)	FF (%)	PCE ^c (%)
D1	P1, 1/2	2.5	80	1.70	0.83	32.8	0.46
D2	P2, 1/2	2.5	80	11.1	0.74	47.7	3.89
D3	P3, 1/2	2.5	80	3.57	0.89	41.5	1.32
D4	P4, 1/2	3.0	85	12.5 (12.2)	0.75	59.0	5.53 (5.40)
D5	P5, 1/2	3.0	80	9.08	0.60	37.1	2.02
D6	P1, 1/2	0.0	21	4.73	0.78	30.2	1.11
D7	P3, 1/2	0.0	21	9.44	0.81	38.4	2.93
D8	P4, 1/2	0.0	85	4.83	0.60	35.2	1.03
D9	P4, 1/3	2.5	85	9.69 (9.31)	0.72	53.2	3.70 (3.55)
D10	P4, 1/1	2.5	85	9.93 (9.92)	0.72	54.8	3.92 (3.92)
D11	P4, 1/2	1.3	85	10.97 (10.81)	0.73	55.2	4.42 (4.36)
D12	P4, 1/2	4.5	85	11.49	0.75	57.6	4.96

^aVolume ratio to o-DCB. ^bDevice fabrication temperature. ^cEQE calibrated data are shown in parentheses.

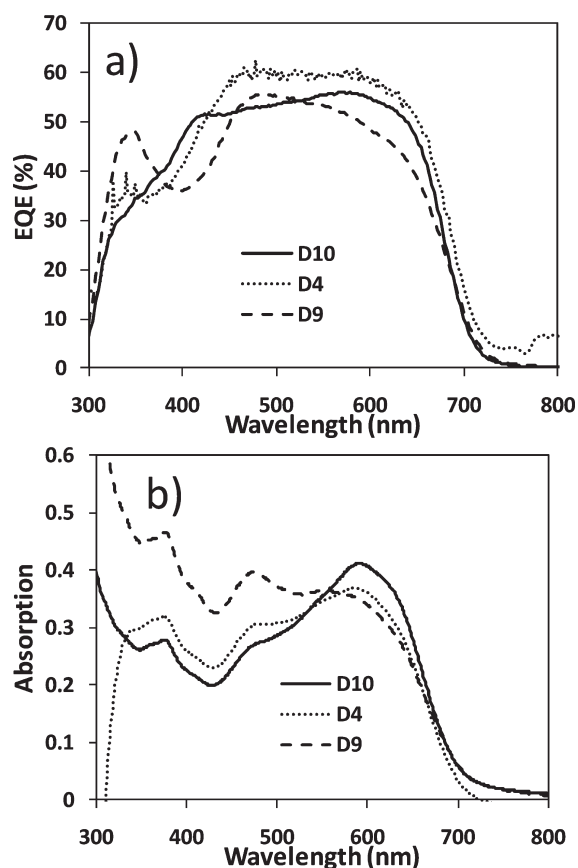


Figure 8. (a) EQE spectra and (b) UV absorption of the active layer of devices D4, D10, and D9.

CONCLUSION

In summary, we synthesized five alternating copolymers of Tz and CPDT with different alkyl side chains (methyl, hexyl, or 2-ethylhexyl) connected to thiophene and CPDT units. Whether using linear or branched side alkyl chains on these two units, especially on the CPDT unit, dramatically affects the solubility, chain stacking, and energy levels of the polymers. These polymers are stable up to 220 °C and will decompose to dinitrile compounds by breaking Tz linkage at 250–300 °C. Polymer solar cells were

fabricated on the basis of the blends of these polymers with PC₇₁BM. Polymer P4, which has all linear hexyl side chains, gives the best performance with a PCE up to 5.53%. The use of DIO as a processing additive improves the device performance for the polymers with poor solubility in the processing solvent, but its influence to the polymers with good solubility is less significant. This effect is closely correlated with the formation of the bicontinuous interpenetrating domain structure, which is confirmed by AFM analysis.

EXPERIMENTAL SECTION

General Methods. NMR spectra were recorded in CDCl₃, acetone-d₆, or o-DCB-d₄ using a Varian Unity Inova spectrometer at a resonance frequency of 399.96 MHz for ¹H and 100.58 MHz for ¹³C. UV–vis spectra were measured using a Varian Cary 5000 spectrometer. Gel permeation chromatography (GPC) (Waters Breeze HPLC system with 1525 Binary HPLC Pump and 2414 differential refractometer) was used to measure the molecular weight and polydispersity index. Chlorobenzene was used as eluent, and commercial polystyrenes were used as standard. The differential scanning calorimetry (DSC) analysis was performed under a nitrogen atmosphere (50 mL/min) using a TA Instrument DSC 2920 at a heating rate of 10 °C/min, calibrated with the melting transition of indium. The thermal gravimetric analysis (TGA) was performed using a TA Instrument TGA 2950 at a heating rate of 10 °C/min under a nitrogen atmosphere (60 mL/min). Cyclic voltammetry (CV) measurements were carried out under argon in a three-electrode cell using 0.1 M Bu₄NPF₆ in anhydrous CH₃CN as the supporting electrolyte. The polymer was coated on the platinum-working electrode. The CV curves were recorded with reference to an Ag quasi-reference electrode, which was calibrated using a ferrocene/ferrocenium (Fc/Fc⁺) redox couple (4.8 eV below the vacuum level) as an external standard. The $E_{1/2}$ of the Fc/Fc⁺ redox couple was found to be 0.40 V vs the Ag quasi-reference electrode. X-ray diffraction (XRD) spectra were recorded on a Bruker AXS D8 Advance instrument with Co K α radiation ($\lambda = 1.789 \text{ \AA}$). Tapping mode AFM images were obtained with a Veeco AFM instrument.

Chemicals. Monomer 4b, 4c, 5a, and 5b were synthesized according to the procedure reported in the literatures.^{10,20,16a}

Synthesis of 4-Methylthiophene-2-carboxaldehyde (1a).

A vacuumed dried 500 mL round-bottomed flask was charged with 3-methylthiophene (9.8 g, 0.10 mol) and anhydrous tetrahydrofuran (200 mL) under argon. The solution was cooled to –78 °C with an acetone/dry ice bath. To the solution was slowly added 2.5 M *n*-butyllithium in hexane (40 mL, 0.10 mol). The reaction solution was stirred

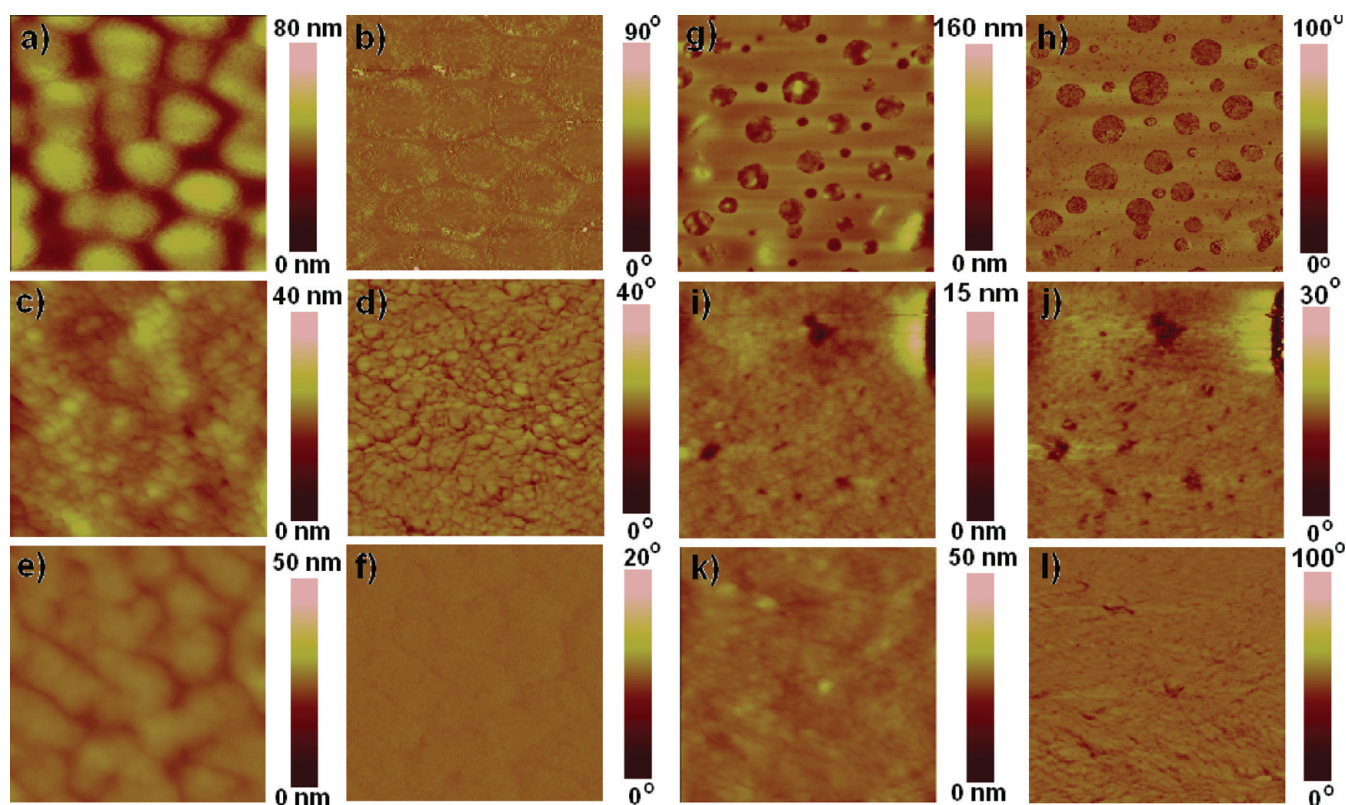


Figure 9. AFM topography (first and third column) and phase (second and fourth column) images of the active layer in devices D6 (a,b), D2 (c,d), D7 (e,f), D8 (g,h,i,j), D9 (k,l). The size of images is $5 \mu\text{m} \times 5 \mu\text{m}$ (g,h) and $500 \text{ nm} \times 500 \text{ nm}$ (for the others).

at -78°C for 30 min before 1-formylpiperidine (12.4 g, 0.11 mol) was added in one shot. Then, the solution was allowed to slowly warm to room temperature and stirred overnight. The solution was poured into ice water (200 mL). The organic layer was separated, and the aqueous layer was extracted with ethyl acetate. The organic phases were combined and washed with distilled water, dried over anhydrous magnesium sulfate, and rotary evaporated to remove the solvent. The liquid residue was subjected to silica-gel column chromatography using ethyl acetate/hexanes (15/85) as eluent to yield a clear liquid product (6.5 g, 52% yield). $^1\text{H NMR}$ (CDCl_3 , δ): 9.86 (s, 1H); 7.56 (d, $J = 1.2$ Hz, 1H); 7.34 (d, $J = 1.2$ Hz, 1H); 2.31 (s, 3H).

Synthesis of 4-Methyl-2-cyanothiophene (1b). A mixture solution of 4-methylthiophene-2-carboxaldehyde (5.1 g, 41 mmol) and hydroxylamine hydrochloride salt (4.0 g, 57.5 mmol) in pyridine/ethanol (30 mL, 1/1, v/v) was stirred at 80°C overnight. After cooling, the solution was rotary evaporated to yield a viscous liquid, which was dissolved in acetic anhydride (30 mL) containing 0.2 g of potassium acetate. The resulting mixture was stirred at 150°C for 4 h. After cooling, the solution was poured into 5% aqueous sodium hydroxide solution and extracted with ethyl acetate. The organic phases were combined and washed with 5% aqueous sodium hydroxide solution until basic. Then the organic phase was washed with distilled water to neutral, dried over anhydrous magnesium sulfate, and rotary evaporated to remove the solvent. The residue was subjected to silica-gel column chromatography to yield a clear light yellow liquid product (3.0 g, 61% yield). $^1\text{H NMR}$ (CDCl_3 , δ): 7.40 (s, 1H); 7.16 (s, 1H); 2.27 (s, 3H). $^{13}\text{C NMR}$ (CDCl_3 , δ): 138.98, 138.40, 128.08, 114.35, 109.21, 15.12.

Synthesis of 3,6-Bis[4-methylthien-2-yl]-s-tetrazine (1c). To a mixture solution of 4-methyl-2-cyanothiophene (17.4 g, 141 mmol) and sulfur (2.24 g, 70.0 mmol) in anhydrous ethanol (20 mL) was added hydrazine monohydrate (99%, 10.5 g, 210 mmol) at room temperature. The solution turned into red, and large amount

of gas evolved. The solution was heated to reflux and stirred for 2 h. After cooling in an ice bath, the resulting red solid was collected and washed with cold ethanol and dried under vacuum. To a solution of the above red solid in chloroform (50 mL) was added isopentyl nitrite (24.6 g, 210 mmol). The resulting solution was stirred at room temperature overnight. The solvent was removed by rotary evaporation, and the red solid residue was washed with ethanol to give pure product (8.7 g, 45% yield). $^1\text{H NMR}$ (CDCl_3 , δ): 8.04 (s, 2H), 7.25 (s, 2H); 2.36 (s, 6H). $^{13}\text{C NMR}$ (CDCl_3 , δ): 161.31, 139.81, 135.52, 132.74, 128.22, 15.70.

Synthesis of 3,6-Bis[4-methyl-5-bromothiophen-2-yl]-s-tetrazine (1d). To a suspension solution of 3,6-bis[4-methylthien-2-yl]-s-tetrazine (3.00 g, 10.9 mmol) in chloroform (80 mL) and acetic acid (25 mL) was added N-bromosuccinimide (5.85 g, 32.8 mmol). The mixture was stirred at 80°C for 4 h, and the resulting solid product was collected by filtration and recrystallized from toluene to give red needle crystals (3.2 g, 68% yield). $^1\text{H NMR}$ (CDCl_3 , δ): 7.92 (s, 2H); 2.29 (6H). $^{13}\text{C NMR}$ (CDCl_3 , δ): 160.79, 139.78, 134.92, 132.38, 118.42, 15.35.

General Procedure for Stille Reaction. To a 25 mL flask was added **4** (0.420 mmol), **5** (0.400 mmol), N,N-dimethylformamide (DMF, 0.5 mL), and toluene (8 mL). The system was purged with Ar under vacuum, and then $(\text{PPh}_3)_4\text{Pd}(0)$ (0.06 g, 0.006 mmol) was added in a glovebox. The solution was stirred and refluxed for 24 h under the protection of Ar. After the solution was cooled to room temperature, the solution was dropped into acetone to precipitate the copolymer. The copolymer was Soxhlet extracted with methanol, acetone, hexanes, and dichloromethane to remove the oligomer and then with chloroform and toluene to obtain the polymer (yield 50–90%). The GPC analysis data are shown in Table 1.

Thermal Decomposition. Polymer **P4** (6.0 mg, 0.0079 mmol) was weighted into a test tube, which was then purged with Ar. Under Ar protection, the tube was placed in a $280\text{--}300^\circ\text{C}$ oil bath for 80 min.

After cooling to room temperature, the crude product (brown oil) was analyzed. $^1\text{H NMR}$ (CHCl_3 , δ): 7.43 (s, 2H), 7.05 (s, 2H), 2.77 (t, $J = 7.8$ Hz, 4H), 1.87 (m, 4H), 1.64 (m, 4H), 1.37 (m, 4H), 1.31 (m, 8H), 1.23–1.10 (br, 12H), 0.99 (m, 4H), 0.88 (t, $J = 6.8$ Hz, 6H), 0.81 (t, $J = 6.8$ Hz, 6H). $^{13}\text{C NMR}$ (CHCl_3 , δ): 159.09, 140.24, 139.45, 139.34, 138.22, 134.47, 122.12, 114.62, 106.46, 54.60, 37.78, 31.79, 31.75, 30.43, 29.79, 29.46, 29.30, 24.80, 22.78, 14.24, 14.21. GPC: $M_n = 720 \text{ g mol}^{-1}$, PDI = 1.03 for the main peak. FT-IR: 2214 cm^{-1} (–CN).

Device Fabrication and Testing. Patterned ITO glass substrates were cleaned with detergent before sonication in CMOS grade acetone and isopropanol for 15 min. The organic residue was further removed by treating with UV–ozone for 10 min. Then a thin layer of PEDOT:PSS (Clevios P, H. C. Starck, 45 nm) was spin coated and dried for 1 h at 120°C . The polymer and PC₇₁BM (ADS) were dissolved in o-DCB containing different amounts of diiodooctane. The solution was filtered and spin coated on top of the PEDOT:PSS layer. Then, 1.0 nm of LiF and 100 nm of Al layer were thermally evaporated through a shadow mask at a pressure of 5×10^{-7} mbar in a Boc Edwards Auto 500 system. The active area is 50 mm^2 . The current–voltage (J – V) characteristics were measured with a Keithley 2400 digital source meter under simulated air mass (AM) 1.5 solar irradiation of 100 mW cm^{-2} (Sciencetech, Inc., SF150). The light intensity was calibrated with a power meter (Gentec Solo PE laser power and energy meter). The external quantum efficiency (EQE) was performed using a Jobin–Yvon Triax 180 spectrometer, a Jobin–Yvon xenon light source, a Merlin lock-in amplifier, a calibrated Si UV detector, and a SR 570 low-noise current amplifier.

AUTHOR INFORMATION

Corresponding Author

*E-mails: zhao.li@nrc-cnrc.gc.ca (Z.L.), jianfu.ding@nrc-cnrc.gc.ca (J.D.).

ACKNOWLEDGMENT

We acknowledge the financial support from NRC-CSIC, NRC-NSERC-BDC and NRC-NANO projects. This work is NRC Publication Number NRCC52846.

REFERENCES

- (1) (a) Clavier, G.; Audebert, P. *Chem. Rev.* **2010**, *110*, 3299. (b) Saracoglu, N. *Tetrahedron* **2007**, *63*, 4199. (c) Kaim, W. *Coord. Chem. Rev.* **2002**, *230*, 126.
- (2) (a) Kim, Y.; Kim, E.; Clavier, G.; Audebert, P. *Chem. Commun.* **2006**, 3612. (b) Kim, Y.; Do, J.; Kim, E.; Clavier, G.; Galmiche, L.; Audebert, P. *J. Electroanal. Chem.* **2009**, *632*, 201.
- (3) Audebert, P.; Miomandre, F.; Clavier, G.; Vernières, M.; Badré, S.; Méallet-Renault, R. *Chem.—Eur. J.* **2005**, *11*, 5667.
- (4) (a) Löbbecke, S.; Pfeil, A.; Krause, H. H.; Sauer, J.; Holland, U. *Propellants, Explos., Pyrotech.* **1999**, *24*, 168. (b) Huynh, M. H. V.; Hiskey, M. A.; Chavez, D. E.; Naud, D. L.; Gilardi, R. D. *J. Am. Chem. Soc.* **2005**, *127*, 12537. (c) Chavez, D. E.; Hiskey, M. A.; Gilardi, R. D. *Angew. Chem., Int. Ed.* **2000**, *39*, 1791.
- (5) (a) Boger, D. L. *Chem. Rev.* **1986**, *86*, 781. (b) Carboni, R. A., Jr.; Lindsey, R. V. *J. Am. Chem. Soc.* **1959**, *81*, 4342.
- (6) Sayed, A. R.; Wiggins, J. S. *Polymer* **2008**, *49*, 2253.
- (7) Sagot, E.; Le Roux, A.; Soulivet, C.; Pasquinet, E.; Poullain, D.; Girard, E.; Palmas, P. *Tetrahedron* **2007**, *63*, 11189.
- (8) Topp, K. D.; Grote, M. *React. Funct. Polym.* **1996**, *31*, 117.
- (9) Audebert, P.; Sadki, S.; Miomandre, F.; Clavier, G. *Electrochem. Commun.* **2004**, *6*, 144.
- (10) Li, Z.; Ding, J.; Song, N.; Lu, J.; Tao, Y. *J. Am. Chem. Soc.* **2010**, *132*, 13160.
- (11) (a) Cheng, Y.-J.; Yang, S.-H.; Hsu, C.-S. *Chem. Rev.* **2009**, *109*, 5868. (b) Dennler, G.; Scharber, M. C.; Brabec, C. J. *Adv. Mater.* **2009**, *21*, 1323. (c) Chen, L.-M.; Hong, Z.; Li, G.; Yang, Y. *Adv. Mater.* **2009**, *21*, 1334. (d) Thompson, B. C.; Fréchet, J. M. J. *Angew. Chem., Int. Ed.* **2008**, *47*, 58. (e) Günes, S.; Neugebauer, H.; Sariciftci, N. S. *Chem. Rev.* **2007**, *107*, 1324. (f) Mayer, A. C.; Scully, S. R.; Hardin, B. E.; Rowell, M. W.; McGehee, M. D. *Mater. Today* **2007**, 28.
- (12) (a) Peet, J.; Kim, J. Y.; Coates, N. E.; Ma, W. L.; Moses, D.; Heeger, A. J.; Bazan, G. C. *Nat. Mater.* **2007**, *6*, 497. (b) Blouin, N.; Michaud, A.; Gendron, D.; Wakim, S.; Blair, E.; Neagu-Plesu, R.; Belletête, M.; Durocher, G.; Tao, Y.; Leclerc, M. *J. Am. Chem. Soc.* **2008**, *130*, 732.
- (13) Moulé, A. J.; Tsami, A.; Bünnagel, T. W.; Forster, M.; Kronenberg, N. M.; Scharber, M.; Koppe, M.; Morana, M.; Brabec, C. J.; Meerholz, K.; Scherf, U. *Chem. Mater.* **2008**, *20*, 4045.
- (14) Smith, K.; Barratt, M. L. *J. Org. Chem.* **2007**, *72*, 1031.
- (15) (a) Pinner, A. *Chem. Ber.* **1893**, *26*, 2126. (b) Abdel-Rahman, M. O.; Kira, M. A.; Tolba, M. N. *Tetrahedron Lett.* **1968**, *9*, 3871. (c) Audebert, P.; Sadki, S.; Miomandre, F.; Clavier, G.; Vernières, M. C.; Saoud, M.; Hapiot, P. *New J. Chem.* **2004**, *28*, 387. (d) Soloducho, J.; Doskocz, J.; Cabaj, J.; Roszak, S. *Tetrahedron* **2003**, *59*, 4761.
- (16) (a) Zhu, Z.; Waller, D.; Gaudiana, R.; Morana, M.; Mühlbacher, D.; Brabec, C. *Macromolecules* **2007**, *40*, 1981. (b) Coffin, R. C.; Peet, J.; Rogers, J.; Bazan, G. C. *Nat. Chem.* **2009**, *1*, 657. (c) Hoven, C. V.; Dang, X.-D.; Coffin, R. C.; Peet, J.; Nguyen, T.-Q.; Bazan, G. C. *Adv. Mater.* **2010**, *22*, E63.
- (17) Oxley, J. C.; Smith, J. L.; Zhang, J. J. *Phys. Chem. A* **2000**, *104*, 6764.
- (18) Jones, B. A.; Facchetti, A.; Marks, T. J.; Wasielewski, M. R. *Chem. Mater.* **2007**, *19*, 2703.
- (19) Lee, J. K.; Ma, W. L.; Brabec, C. J.; Yuen, J.; Moon, J. S.; Kim, J. Y.; Lee, K.; Bazan, G. C.; Heeger, A. J. *J. Am. Chem. Soc.* **2008**, *130*, 3619.
- (20) Ding, J.; Song, N.; Li, Z. *Chem. Commun.* **2010**, 46, 8668.